MECSOL 2022 - Proceedings of the 8th International Symposium on Solid Mechanics
M.L. Bittencourt, J. Labaki, L.C.M. Vieira Jr. and E. Mesquita (Editors), Campinas SP, Brazil, October 17th to 19th, 2022

Homogenization and metamaterials: an effective alliance

Claudia Comi[1], David Faraci[1] , Marco Moscatelli[1] and Jean-Jacques Marigo[2]

[1] Department of Civil and Environmental Engineering, Politecnico di Milano, Piazza L. da Vinci 32, 20133 Milano (Italy)
[2] Laboratoire de Mécanique des Solides, École Polytechnique, Route de Saclay, 91129 Palaiseau (France)

Abstract. The fast growing field of metamaterials opens a number of new opportunities and applications but, at the same time, introduces many challenges in the design and modeling. The two scale asymptotic homogenization appears as a promising tool for the design and optimization of systems composed of metamaterials. In this contribution, we discuss the role of homogenization in the development of practical applications of metamaterials. Focus will be in particular on two significant examples: the optimization of auxetic metamaterials for energy absorption and the design of a system for energy localization that includes locally resonant materials. In both cases, the metamaterial is substituted with an equivalent homogenized continuum allowing for a fast parametric optimization and leading to a significant computational advantage.

Keywords: asymptotic homogenization, auxetic material, locally resonant material, effective mass, energy harvesting

INTRODUCTION

Metamaterials are the results of the long lasting effort of physicists, material scientists, and engineers to go beyond ("meta") what nature has given to us in terms of materials properties. The search enhancement can be in the directions of stronger, tougher, or lighter materials or in the peculiar dynamic behaviour with vibration isolation or wave focusing properties.

The fabrication of metamaterials, often periodic, with complex microstructure, is nowadays possible thanks to significant technological advances in micro-lithography, three-dimensional printing and multi-photon polymerization (Zega et al. (2022), Cang et al. (2022)).

One class of micro-structured materials that could provide advantages over conventional materials is that of auxetic materials discovered by Lakes in 1987 (Lakes (1987)). These materials have a negative Poisson's ratio, ν, which means that they expand in the lateral direction when stretched longitudinally. This property leads to improved indentation resistance, thermal shock resistance, impact performance (Faraci et al. (2021), Madke and Chowdhury (2020)), fracture toughness and fatigue behaviour in tension (Bezazi and Scarpa (2009)). Figure 1a shows an example of a 3-dimensional lattice of an auxetic metamaterial, with the unit cell shown in Fig. 1b.

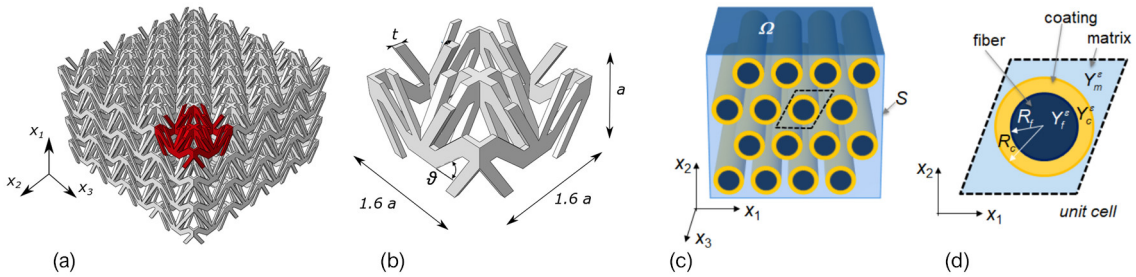

Figure 1: Metamaterials, (a) three-dimensional lattice of an auxetic material, (b) corresponding unit cell, (c) two-dimensional lattice of a locally resonant material, (d) corresponding unit cell.

Another wide class of metamaterials is represented by phononic crystals (PnCs), first introduced in (Kushwaha et al. (1993)). Their interest stems from the possibility to manipulate wave propagation by properly varying the elastic properties of structured materials. Frequency band gaps can appear in the propagation of acoustic (or elastic) waves if the material's elastic properties, elastic moduli and/or density, are properly periodically designed (Laude (2015)). The interference of incident and reflected elastic waves occurs when the wavelength of waves is comparable to the lattice spacing, giving

rise to the appearance of Bragg-like gap. In (D'Alessandro et al. (2018)) auxeticity and phononic crystals bandgap properties are properly combined to obtain a single phase periodic structure with a wide tunable bandgap. Another opening mechanism of band gap is associated with the coupling between the propagating wave and local resonances inside the unit cells of the periodic material, in this latter case PnCs are also called locally resonant materials (LRMs) (Zhou et al. (2012), Moscatelli et al. (2019)). Figure 1c shows an example of a three-components LRM with two-dimensional periodicity.

Due to the complex structure of metamaterials, the optimization of their geometry and composition to achieve target properties and the prediction of structural behavior require time consuming calculations (see e.g. Krushynska et al. (2014), Comi and Driemeier (2018)). The two-scale homogenization approach represents an alternative effective tool to tackle problems involving metamaterials. This approach was first proposed in Auriault and Bonnet (1985) for high-contrast binary elastic composite materials in the long wavelength regime, and then developed in different directions (Craster et al. (2010), Auriault and Boutin (2012), Pham et al. (2017), Comi and Marigo (2020), Comi et al. (2019)).

In this paper, we highlight the role of the asymptotic homogenization in the development of practical applications of metamaterials. After a section summarizing the two-scale homogenization approach for periodic materials, we will focus on two specific examples. The first concerns the optimization of auxetic metamaterials for energy absorption and the use of homogenization to simulate the behavior of a protective sandwich plate with an auxetic core for impact absorption. The second example concerns the design of a system for energy localization that includes barriers of locally resonant materials. In both cases the metamaterial is substituted with an equivalent homogenized continuum: this opens the way to fast parametric optimization and leads to significant computational advantage.

TWO SCALE ASYMPTOTIC HOMOGENIZATION

Let us consider a continuum domain Ω of characteristic size L, e.g., the one represented in Figure 1c, which is characterized by the periodic repetition of a unit cell Y^ϵ (Figure 1d) of characteristic size $\ell \ll L$. This hypothesis of separation of scales allows to develop the solution in terms of the small parameter $\epsilon = \ell/L$. We assume that the periodic body is made of a connected stiff matrix (m) and rigid inclusions (f) which are coated by a soft material (c). The propagation of elastic waves within Ω is governed by the Helmholtz equation

$$\operatorname{div}\left[\mathbb{D}^\epsilon : \boldsymbol{\varepsilon}(\mathbf{u}^\epsilon)\right] + \rho^\epsilon \omega^2 \mathbf{u}^\epsilon = \mathbf{0} \qquad \text{in } \Omega, \tag{1}$$

where $\mathbf{u}^\epsilon$ is the displacement field, ω is the angular frequency, ρ^ϵ is the mass density, $\boldsymbol{\varepsilon}$ is the small strain tensor, i.e., the symmetric part of the displacement gradient and $\mathbb{D}^\epsilon$ is the fourth-order elastic stiffness tensor. For isotropic materials the stiffness tensor can be expressed as

$$\mathbb{D}^\epsilon = 2\mu^\epsilon \mathbb{I} + \lambda^\epsilon \mathbf{I} \otimes \mathbf{I}, \tag{2}$$

with $\lambda^\epsilon, \mu^\epsilon$ the Lame's constants of the constituent materials. As for the properties of the material constituents we assume

$$\lambda^\epsilon = \begin{cases} \lambda_m & \text{in } Y_m^\epsilon \\ \epsilon^2 \lambda_c & \text{in } Y_c^\epsilon \end{cases}, \qquad \mu^\epsilon = \begin{cases} \mu_m & \text{in } Y_m^\epsilon \\ \epsilon^2 \mu_c & \text{in } Y_c^\epsilon \end{cases}, \qquad \text{and} \qquad \rho^\epsilon = \begin{cases} \rho_m & \text{in } Y_m^\epsilon \\ \rho_c & \text{in } Y_c^\epsilon \\ \rho_f & \text{in } Y_f^\epsilon \end{cases}, \tag{3}$$

with λ_m, μ_m and ρ_m of the same order of magnitude of λ_c, μ_c and ρ_c (and ρ_f), respectively.

The two-scale homogenization allows for the determination of the effective homogenized properties of the periodic media by studying the asymptotic behaviour of (1) as $\epsilon \to 0$. Denoting by $\mathbf{x}$ the macroscopic variable, we introduce the re-scaled unit cell $Y = Y^\epsilon/\epsilon$, the fast variable $\mathbf{y} = \mathbf{x}/\epsilon$ and we assume the following expansion of the displacement field

$$\mathbf{u}^\epsilon(\mathbf{x}) = \mathbf{u}^0\left(\mathbf{x}, \frac{\mathbf{x}}{\epsilon}\right) + \epsilon\, \mathbf{u}^1\left(\mathbf{x}, \frac{\mathbf{x}}{\epsilon}\right) + \ldots, \tag{4}$$

where the vectors $\mathbf{u}^i(\mathbf{x}, \mathbf{y})$ are defined on $\Omega \times Y$ and are periodic with respect $\mathbf{y}$.

Substituting (4) in the governing equation (1) one obtain a sequence of differential problem for each order of the parameter ϵ. It is possible to prove, see Comi and Marigo (2020) for the complete derivation, that the homogenized Helmholtz equation at order 0 reads

$$\operatorname{div}_{\mathbf{x}}(\mathbb{D}^0 : \boldsymbol{\varepsilon}_{\mathbf{x}}(\mathbf{U}_m^0)) + \omega^2 \boldsymbol{\rho}^0(\omega) \cdot \mathbf{U}_m^0 = \mathbf{0} \qquad \text{in } \Omega, \tag{5}$$

where $\mathbf{U}_m^0(\mathbf{x})$ is the $0-$th order displacement in the matrix, which turns to be independent on $\mathbf{y}$, and $\mathbb{D}^0$ is the homogenized stiffness tensor. The stiffness components can be evaluated through

$$D_{ijhk}^0 = \frac{1}{|Y|} \int_{Y_m} \left[\boldsymbol{\varepsilon}_{\mathbf{y}}(\boldsymbol{\chi}^{ij}) + \mathbf{e}_i \odot \mathbf{e}_j\right] : \mathbb{D}_m : \left[\boldsymbol{\varepsilon}_{\mathbf{y}}(\boldsymbol{\chi}^{hk}) + \mathbf{e}_h \odot \mathbf{e}_k\right] \, d\mathbf{y}, \tag{6}$$

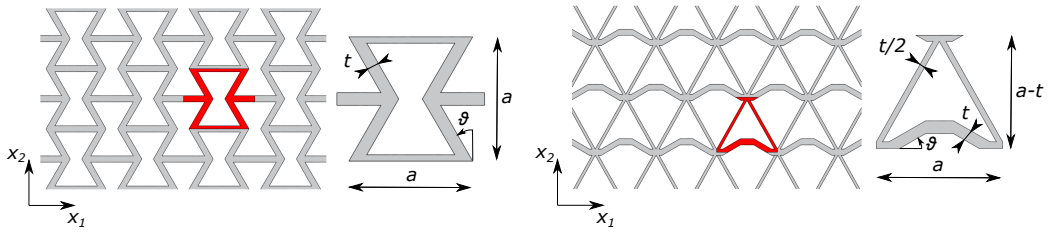

(a) (b)

Figure 2: Two-dimensional (a) RHC lattice with its unit cell, (b) RT lattice with its unit cell.

$\mathbf{e}_i$ being the unit vector in the $i-$th direction. The functions $\boldsymbol{\chi}^{ij}(\mathbf{y})$ in (6) are the solution of the so-called matrix cell problems

$$\begin{cases} \mathrm{div}_{\mathbf{y}}\left[\mathbb{D}_m : \boldsymbol{\varepsilon}_{\mathbf{y}}(\boldsymbol{\chi}^{ij})\right] = \mathbf{0} & \text{in } Y_m \\ \boldsymbol{\chi}^{ij} \quad \text{periodic} & \text{on } \partial Y \\ \left[\mathbb{D}_m : \left(\boldsymbol{\varepsilon}_{\mathbf{y}}(\boldsymbol{\chi}^{ij}) + \mathbf{e}_i \odot \mathbf{e}_j\right)\right] \cdot \mathbf{n} \quad \text{anti-periodic} & \text{on } \partial Y \\ \left[\mathbb{D}_m : \left(\boldsymbol{\varepsilon}_{\mathbf{y}}(\boldsymbol{\chi}^{ij}) + \mathbf{e}_i \odot \mathbf{e}_j\right)\right] \cdot \mathbf{n} = \mathbf{0} & \text{on } \partial Y_m \setminus \partial Y \end{cases}, \tag{7}$$

where $\mathbf{n}$ is the outside normal to the boundary. Equations (7) represent elastic problems in which uniform eigenstrains are imposed within the unit cell with cavities instead of the coated inclusions. Note that the above expression also holds when the inclusions are replaced by voids, as for the lattice in Figure 1a.

The term $\boldsymbol{\rho}^0(\omega)$ in equation (5) represents the effective mass density of the periodic media, which turns out to be a frequency-dependent tensor. Its components can be evaluated on the basis of coating cell problems and by enforcing the global dynamic equilibrium of the rigid inclusion.

For simplicity sake, as done by Comi et al. (2019), we consider a system with 2-dimensional periodicity with cylindrical inclusions of radius R_f and annular coatings of external radius R_c, as depicted in Figure 1c. In the simple case of anti-plane shear wave propagation, the effective mass density reduces to a scalar and can be evaluated through

$$\rho^0 = \rho_m \frac{|Y_m|}{|Y|} + \frac{\rho_c}{|Y|}\int_{Y_c} \eta \, d\mathbf{y} + \rho_f \frac{|Y_f|}{|Y|}\,\eta(R_f) \tag{8}$$

The function $\eta(\mathbf{y})$ is given by

$$\eta(\mathbf{y}) = \frac{\lambda R_f \rho_f \left(J_0(\kappa r)Y_0(\kappa R_f) - J_0(\kappa R_f)Y_0(\kappa r)\right) + 2\rho_c \left(J_1(\kappa R_f)Y_0(\kappa r) - J_0(\kappa r)Y_1(\kappa R_f)\right)}{\kappa R_f \rho_f \left(J_0(\kappa R_c)Y_0(\kappa R_f) - J_0(\kappa R_f)Y_0(\kappa R_c)\right) + 2\rho_c \left(J_1(\kappa R_f)Y_0(\kappa R_c) - J_0(\kappa R_c)Y_1(\kappa R_f)\right)}, \tag{9}$$

where $r = ||\mathbf{y}||$, $\kappa^2 = \rho_c\omega^2/\mu_c$, J_0 and J_1 are Bessel functions of the first kind and Y_0 and Y_1 are Bessel functions of second kind.

AUXETIC METAMATERIALS FOR IMPACT ABSORPTION

Parametric optimization of auxetic metamaterials

The homogenization method described in the previous section allows for the computation of the homogenized properties of linear-elastic periodic materials. This procedure can be employed as a fast and efficient tool for the parametric study of the effective properties of metamaterials, helpful in the design phase.

As an example, we consider two different periodic materials, in plane strain condition, made of a single-phase, i.e., constituted only by the matrix, which elastic properties are $E_m = 480$ MPa and $\nu_m = 0.48$. The re-entrant honeycomb lattice (RHC), shown in Figure 2a with its unit cell, and the re-entrant triangle (RT) lattice, depicted in Figure 2b with its unit cell, are analyzed. Both geometries are characterized by three parameters that control the size a of the cells, the thickness t of the walls and the angle $\vartheta > 0$ of inclination of the re-entrant branches.

For each possible combination of t/a and ϑ, one can solve the matrix cell problems (7) and evaluate through (6) the homogenized stiffness tensor $\mathbb{D}^0$. It should be noticed, in general, that the homogenized material is anisotropic, even if

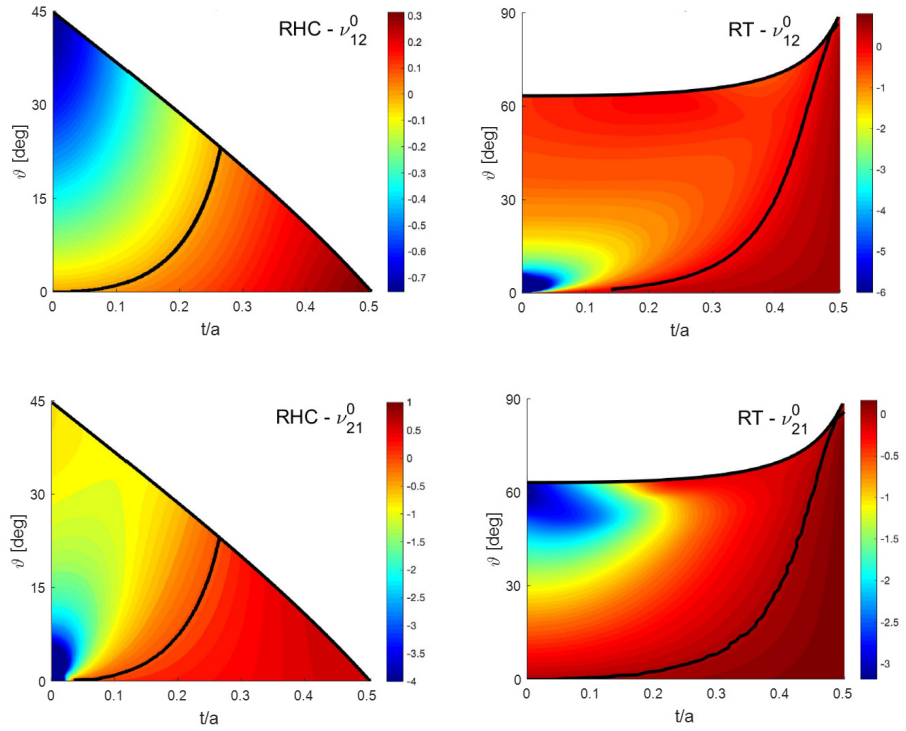

Figure 3: Contours of the effective in-plane Poisson's ratios for the RHC lattice (left) and RT one (right) as function of the ratio t/a and ϑ.

the constituent material is isotropic. For this reason, one must consider the in-plane effective Poisson's ratios

$$\nu_{12}^0 = -\frac{C_{1122}^0}{C_{1111}^0} \qquad \text{and} \qquad \nu_{21}^0 = -\frac{C_{1122}^0}{C_{2222}^0}, \tag{10}$$

being $\mathbb{C}^0$ the effective compliance tensor, i.e., the inverse tensor of $\mathbb{D}^0$.

Figure 3 shows the contour plots of ν_{12}^0 and ν_{21}^0 for the RHC lattice (on the left) and the RT one (on the right), against the ratio t/a and the re-entrant angle ϑ. Note that each contour has different scale colours in order to highlight their variability. The white regions correspond to combinations of the geometric parameters that are not admissible as they would provoke interpenetration between the walls of the lattices.

The black line within the contours divides the region where the material behaves traditionally ($\nu^0 > 0$) from the one in which the auxetic behaviour manifests ($\nu^0 < 0$). In particular, it can be observed that for a fixed value of the re-entrant angle ϑ, the Poisson's ratios tend to decrease as the ratio t/a becomes smaller.

Protective auxetic sandwich plate

The linear homogenization method can be also employed to reduce the computational burden of numerical analyses of metamaterials, especially when the size of the microstructure is orders of magnitude lower with respect to the dimension of the model. This situation occurs e.g. for the proposal in Faraci et al. (2021) of a wearable protective mask against impact having a layered structure with a metamaterial core. Modeling the entire mask with the actual microstructure would require prohibitive computational times. As in Faraci et al. (2021), we hence simulate by finite element analysis the impact of a rigid sphere against just a small portion of the sandwich structure (Figure 4a) composed of two homogeneous layers and the auxetic material core shown in Figure 1a, of $5 \times 5 \times 4$ cells made of a linear-elastic material.

A typical deformation of the (half) device is shown in Figure 4b, highlighting the strong nonlinearities that occur in the neighbourhood of the impact region, like buckling phenomena and the self-contact between the branches of the metamaterial. In the same figure, the time evolution of the force transmitted on the bottom surface of the protective device during the impact is reported with a blue curve.

The presence of many non-linear phenomena prevents from the use of homogenization. However, since these non-

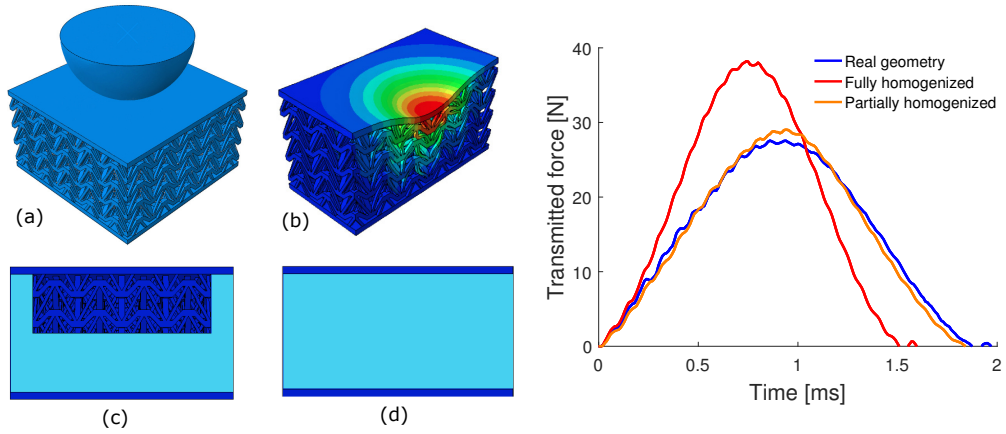

Figure 4: Left part: (a) real geometry with the impacting (half) sphere; (b) typical deformation of the mask; model for the partially (c) and fully (d) homogenized mask. Right part: transmitted force versus time for the three different models.

linear effects are localized, one could think to replace, with the equivalent linear continuum, only the portion of the protective device which is far away from the impact region, as shown in Figure 4c, i.e., where the hypothesis of linear behaviour is quite reasonable. The relative transmitted force (in orange) is in good agreement with the real one. The peak force is estimated with an error of 5%, with a saving of 50% of computational time, already for this very small portion of the mask. A considerably higher computation gain would be obtained for the whole system.

As expected, the analysis where the metamaterial core is completely substituted by an equivalent homogenous media having the same effective linear-elastic properties, see Figure 4d, leads to a completely different transmitted force response, see the red curve.

LOCALLY RESONANT MATERIAL WITH DEFECTS

The dynamic behavior of LRMs of the type shown in Figure 1c is generally characterized by sub-wavelength bandgaps. This feature makes them useful for energy harvesting applications, with the aim of scavenging electrical energy from ambient vibrations, that are indeed generally characterized by a low-frequency content. These sources of mechanical energy are often broadly distributed in space. Therefore, to improve the efficiency of an energy harvesting device, LRMs can be exploited by limiting the propagation of waves in a compact region, to trap and focus the energy produced by external vibrations.

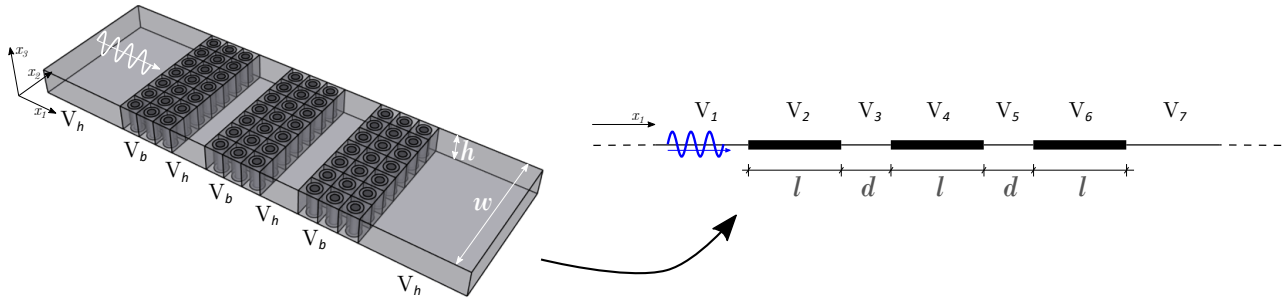

Figure 5: On the left, the system for mechanical energy harvesting. Parts V_b are composed of the LRM shown in figure 1c. Parts V_h are made up of the material used for the matrix Y_m. On the right the 1D domain resulting from the application of the homogenization of parts V_b.

When a defect of periodicity or a cavity is introduced in a LRM, so-called defect modes can appear at frequencies belonging to a bandgap, with the corresponding field being localized around the defect or cavity and decaying exponentially outside it (Moscatelli et al., 2021). This peculiar behavior is here analyzed by considering a configuration similar to that

used in Moscatelli et al. (2020a,b) and represented in Figure 5.

With respect to the previous works, we show how the addition of a second resonant cavity generates two defect modes inside the first bandgap of the LRM under consideration. Specifically, we look for optimal cavities width, corresponding to a maximum of energy localization, for a varying working frequency. By substituting the metamaterial parts (V_b) with the corresponding homogenized material, characterized by the effective properties (6) and (8), the computation time of this parametric study reduces to a few seconds. A numerical solution of the actual problem would require a much larger effort.

Problem definition

Let us consider the system depicted in Figure 5. The LRM shown in Figure 1c is used for parts V_b, while parts V_h are composed of the homogeneous material employed for the matrix Y_m. The LRM is thus split in three parts by two cavities. We consider an incoming wave, polarized along x_3 direction, propagating in x_1 direction, with a wave length $L \gg \ell$. Both the height h and the width w of the system are much greater than L. Our aim is that of optimizing the system to maximize the energy localization in the two cavities.

By exploiting the previous derivation of the effective material properties, the LRM can be substituted with its homogenized counterpart. Accordingly, the problem can be reduced to a scalar wave propagation problem, along direction x_1, across a 1D system composed of 7 homogeneous domains V_j with $j = \{1,\dots,7\}$ (c.f. Figure 5). For a fixed frequency inside a bandgap of the LRM, the motion is governed by the following equations:

$$\begin{cases} u''(x_1) + k^2 u(x_1) & \text{in } V_h \\ u''(x_1) - s^2 u(x_1) & \text{in } V_b \end{cases} \quad \text{with} \quad k^2 = \omega^2 \frac{\rho_m}{\mu_m}, \quad s^2 = \omega^2 \frac{|\rho^0|}{\mu^0}, \tag{11}$$

where u denotes a displacement along x_3, μ^0 is the first order homogenized shear modulus, obtained from relation (6) and ρ^0 is the effective mass density defined in (8) .

The negative sign in the second of equations (11) is due to the fact that the effective mass density ρ^0 is negative for frequencies inside a bandgap (Comi et al., 2019). General solutions of (11) can be searched as:

$$\begin{cases} U_h(x) = A_h \exp\{-\mathrm{i}kx\} + B_h \exp\{\mathrm{i}kx\} & \text{in } V_h, \\ U_b(x) = A_b \cosh\{sx\} + B_b \sinh\{sx\} & \text{in } V_b. \end{cases}$$

By considering perfect interfaces between the different parts composing the system, continuity of displacements and stresses can be imposed and the motion can be derived in closed-form. The coefficients A_h, B_h and A_b, B_b are thus known inside each of the 7-th domains composing the system. The mechanical energy density e_h of the two cavities, averaged in time over a period, is finally obtained using the following relation

$$\langle e_h \rangle = \frac{\mu_h k^2}{2} \left[|A_h|^2 + |B_h|^2 \right], \tag{12}$$

where $\langle(\bullet)\rangle$ denotes the average in time of $(\bullet)$.

Optimization of energy localization

Let us here analyze a specific case. For this, we consider a squared lattice with unit cells of side $a = 1$ mm, with a coating layer Y_c of external radius $R_c = 0.415a$, and an inner fiber Y_f of radius $R_f = 0.7R_c$. We fix the material properties as in table 1 and we consider 40 unit cells along x_1 across parts V_2, V_4 and V_6. Specifically, the LRM here used is

Table 1: Material properties.

Constituents	E [MPa]	ν [-]	ρ [Kg/m^3]
Y_m (epoxy)	3600	0.370	1180
Y_c (rubber)	0.118	0.469	1300
Y_f (lead)	14000	0.420	11340

characterized by a first bandgap between 2.4 and 5.7 KHz. From relation (12), the averaged mechanical energy density

$\langle e_h \rangle$ in the two cavities, normalized with respect to the energy in part V_1, can be computed for frequencies belonging to the first bandgap of the LRM and for a varying width of the cavities. The result is given in the contour plots depicted in Figure 6, where the left panels refer to the cavity V_3 and the right panels to V_5.

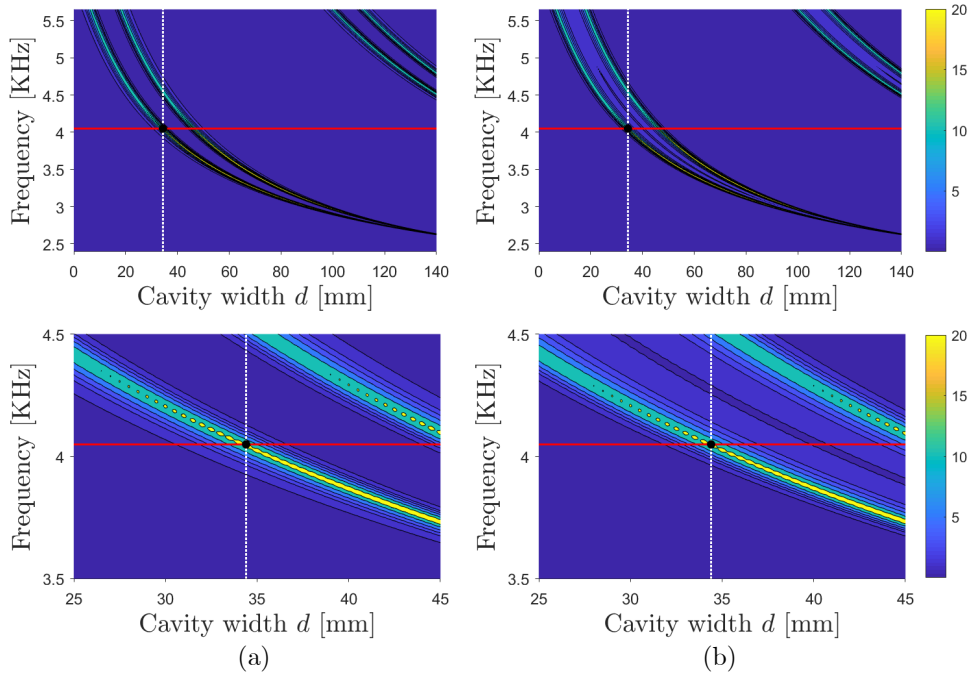

Figure 6: Averaged mechanical energy density $\langle e_h \rangle$ in the cavities V_3 (left panels) and V_5 (right panels), normalized with respect to the energy in part V_1. A zoom of the contour plots in the first row around a width of 33.7 mm is given in the second row. The contour plots are obtained exploiting the homogenization technique.

By fixing a working frequency (red horizontal line), one can pick from the contour plots the optimal width for the cavities (white vertical dotted line), corresponding to a maximum of localization of the mechanical energy. The second row in Figures 6a and 6b show a close-up view of the contours near the selected point: one can observe that when the energy is maximum in one of the two cavities, it is also maximum in the other one. Accordingly, the energy $\langle e_h \rangle$ is localized and maximum in both cavities at the same time. Moreover, once an optimal width is fixed, a second peak at a frequency close to the working one is found. From a harvesting point of view, this can be advantageous when the frequency content of the external vibration is spread around the working frequency fixed for the design of the system.

This behavior is further confirmed by comparing the results from the homogenization approach, with those coming from a numerical solution of the problem. Let us consider the averaged energy in the two cavities for frequencies varying in the first bandgap, by fixing an optimal width d. More specifically, we here optimize the system for an incoming wave at the frequency indicated by the red horizontal line in Figure 6 (4.07 kHz). We then select the first (optimal) width of 33.7 mm for both cavities (indicated by a white dotted line in the figure).

The averaged energy, normalized with that in part V_1, is reported in Figure 7 for the cavity V_3 (panel (a)) and V_5 (panel (b)). The numerical evaluation of the averaged energy (blue curve) is in good agreement with the prediction obtained by exploiting the homogenization technique (orange curve). The homogenization is thus able to exactly characterize the response of the system and can be efficiently used for the design of an energy harvester of the type analyzed in the present work.

CONCLUSIONS

The two scale asymptotic homogenization approach can be effectively used in various problems involving micro-structured periodic materials. Under the hypothesis of separation of scales and linear behavior the metamaterial can be substituted by an equivalent homogeneous system and this opens the way to the optimization of the material itself and of the structure. It was shown that, even though the full microstructure must be considered where non linear phenomena occur, homogenization can still be useful to homogenize the system far from critical zones. When locally resonant

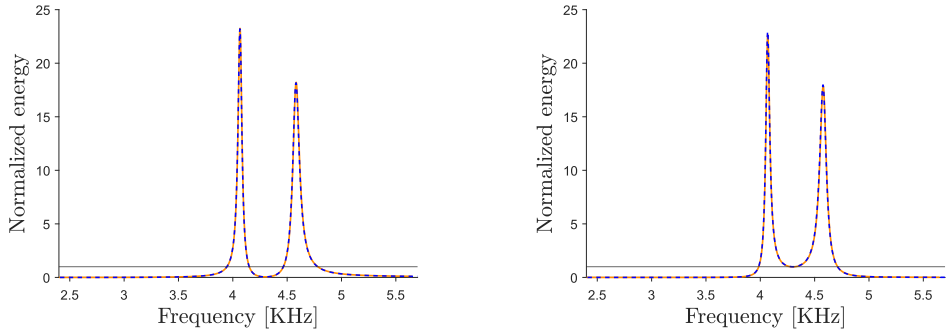

(a) (b)

Figure 7: Averaged mechanical energy density in the cavities V_3 (a) and V_5 (b), normalized with the energy in part V_1. The orange curves are obtained from the homogenization approach, while the blue dashed curves from a finite element analysis.

materials are considered, under the hypothesis of high contrast between the constituents and in the long wave length limit, the homogenization approach allows to compute in close form the band-gaps as the intervals of negative effective mass density. Using this property an energy harvesting system employing LRMs with cavities was proposed and optimized in order to maximize the energy localization inside the cavities.

ACKNOWLEDGMENTS

The Authors acknowledge the contribution of the student Julien Blondiau in the numerical simulations of auxetic materials.

REFERENCES

Auriault, J.-L. and G. Bonnet (1985). Dynamique des composites élastiques périodiques. *Arch.Mech. 37*(January 1985), 269–284.

Auriault, J.-L. and C. Boutin (2012). Long wavelength inner-resonance cut-off frequencies in elastic composite materials. *Int. J. Solids Struct. 49*(23-24), 3269–3281.

Bezazi, A. and F. Scarpa (2009). Tensile fatigue of conventional and negative Poisson's ratio open cell PU foams. *International Journal of Fatigue 31*(3), 488–494.

Cang, Y., Y. Jin, B. Djafari-Rouhani, and G. Fytas (2022). Fundamentals, progress and perspectives on high-frequency phononic crystals. *Journal of Physics D: Applied Physics 55*(19), 193002.

Comi, C. and L. Driemeier (2018). Wave propagation in cellular locally resonant metamaterials. *Latin American Journal of Solids and Structures 15*(4), 1–15.

Comi, C. and J.-J. Marigo (2020, apr). Homogenization Approach and Bloch-Floquet Theory for Band-Gap Prediction in 2D Locally Resonant Metamaterials. *J. Elast. 139*(1), 61–90.

Comi, C., M. Moscatelli, and J.-J. Marigo (2019). Two scale homogenization in ternary locally resonant metamaterials. *Mater. Phys. Mech. 44*, 8–18.

Craster, R. V., J. Kaplunov, and J. Postnova (2010). High-frequency asymptotics, homogenisation and localisation for lattices. *Q. J. Mech. Appl. Math. 63*(4), 497–519.

D'Alessandro, L., V. Zega, R. Ardito, and A. Corigliano (2018). 3D auxetic single material periodic structure with ultra-wide tunable bandgap. *Scientific Reports 8*(1), 1–9.

Faraci, D., L. Driemeier, and C. Comi (2021). Bending-Dominated Auxetic Materials for Wearable Protective Devices Against Impact. *Journal of Dynamic Behavior of Materials 7*(3), 425–435.

Krushynska, A. O., V. G. Kouznetsova, and M. G. Geers (2014). Towards optimal design of locally resonant acoustic metamaterials. *Journal of the Mechanics and Physics of Solids 71*(1), 179–196.

Kushwaha, M. S., P. Halevi, L. Dobrzynski, and B. Djafari-Rouhani (1993, Sep). Acoustic band structure of periodic elastic composites. *Phys. Rev. Lett. 71*, 2022–2025.

Lakes, R. (1987). Foam structures with a negative poisson's ratio. *Science 235*(4792), 1038–1040.

Laude, V. (2015, jan). *Phononic Crystals*. Berlin, München, Boston: DE GRUYTER.

Madke, R. R. and R. Chowdhury (2020). Anti-impact behavior of auxetic sandwich structure with braided face sheets and 3D re-entrant cores. *Composite Structures 236*(October 2019), 111838.

Moscatelli, M., R. Ardito, L. Driemeier, and C. Comi (2019, aug). Band-gap structure in two- and three-dimensional cellular locally resonant materials. *J. Sound Vib. 454*, 73–84.

Moscatelli, M., C. Comi, and J.-J. Marigo (2020a). Locally Resonant Materials for Energy Harvesting at Small Scale. In *Proc. XXIV AIMETA Conf. 2019*, Number September, pp. 606–626. Rome.

Moscatelli, M., C. Comi, and J.-J. Marigo (2020b). Locally resonant materials for energy harvesting at small scale. In A. Carcaterra, A. Paolone, and G. Graziani (Eds.), *Proceedings of XXIV AIMETA Conference 2019*, pp. 606–626. Springer.

Moscatelli, M., C. Comi, and J.-J. Marigo (2021, jul). On the dynamic behaviour of discrete metamaterials: From attenuation to energy localization. *Wave Motion 104*, 102733.

Pham, K., A. Maurel, and J. J. Marigo (2017, sep). Two scale homogenization of a row of locally resonant inclusions - the case of anti-plane shear waves. *J. Mech. Phys. Solids 106*, 80–94.

Zega, V., L. Pertoldi, T. Zandrini, R. Osellame, C. Comi, and A. Corigliano (2022). Microstructured Phononic Crystal Isolates from Ultrasonic Mechanical Vibrations. *Applied sciences 12*, 1–12.

Zhou, X., X. Liu, and G. Hu (2012). Elastic metamaterials with local resonances: an overview. *Theor. Appl. Mech. Lett. 2*(4), 041001.

RESPONSIBILITY NOTICE

The authors are the only parties responsible for the printed material included in this paper.